Adaptive-boost molecular dynamics simulation of carbon diffusion in iron

Akio Ishii, Shigenobu Ogata,* and Hajime Kimizuka
Department of Mechanical Science and Bioengineering, Osaka University, Osaka 560-8531, Japan

Ju Li†
Department of Nuclear Science and Engineering and Department of Materials Science and Engineering, Massachusetts Institute of Technology, Cambridge, Massachusetts 02139, USA

(Received 4 April 2011; revised manuscript received 1 December 2011; published 21 February 2012)

We have developed an accelerated molecular dynamics (MD) method to model atomic-scale rare events. In this method, a smooth histogram of collective variables is first estimated by canonical ensemble molecular dynamics calculations, and then a temperature-dependent boost potential is iteratively constructed to accelerate the MD simulation. This method not only allows us to observe the rare events but also to evaluate the profile of free energy and trial frequency along the reaction coordinate. We employed this method to study carbon diffusion in bcc iron and evaluated carbon's temperature-dependent diffusivity. The obtained diffusivities agree well with the experimental measurements. Even at low temperature for which, to the best of our knowledge, no experimental data are available, the diffusivity can be evaluated accurately. Additionally, we study carbon diffusion inside the edge dislocation core in bcc iron, and demonstrate the applicability of the method to rare events on a rugged free-energy surface.

DOI: 10.1103/PhysRevB.85.064303 PACS number(s): 82.20.Db, 02.70.Ns, 61.72.jj

I. INTRODUCTION

Using the discrete atomic positions $\boldsymbol{r} \equiv \{\boldsymbol{r}_1, \ldots, \boldsymbol{r}_N\}$ as the degrees of freedom and an interatomic potential $V(\boldsymbol{r})$, atomistic simulation is a powerful approach for understanding and predicting materials behavior. Molecular dynamics (MD), a conventional atomistic simulation method, provides a detailed atomic trajectory $\boldsymbol{r}(t)$ and information regarding the thermodynamics and "fast" dynamics of solids. However, MD is not suitable for understanding thermomechanical rare events with large activation energy barriers because of the computational cost, which limits MD's time duration to ∼ns. Many microscopic events of interest in solids, such as diffusion,[1] may occur with an average waiting time of seconds or more. Therefore, there are strong demands for the development of methods that can help investigate rare microscopic events. So far, several closely related methods have been proposed: local elevation,[2] conformational flooding,[3] umbrella potential,[4] hyperdynamics,[5] metadynamics,[6] bond boost,[7] strain boost,[8] etc. By adding a boost potential $\Delta V(\boldsymbol{r})$ to the Hamiltonian, the activation-energy barriers for rare events are lowered and their occurrences are accelerated by a common factor, which can be estimated based on the transition state theory (TST).[5]

II. ADAPTIVE-BOOST METHOD

Here, we have developed a general adaptive-boost formalism based on previous developments.[2–8] Given a uncharacterized $V(\boldsymbol{r})$, we first evaluate the smooth histogram $\rho(\boldsymbol{A})$ of collective variables (CVs)[9,10] $\boldsymbol{A} \equiv \{A_1(\boldsymbol{r}), \ldots, A_M(\boldsymbol{r})\}$ by MD, and then utilize the smooth histogram (probability density) of $\boldsymbol{A}$ as the boost potential

$$\Delta V(\boldsymbol{r}) \propto k_{\mathrm{B}} T \ln \rho(\boldsymbol{A}) \tag{1}$$

in subsequent accelerated MD simulations. In terms of the formal justification for this dynamics, it is entirely identical to hyperdynamics,[5] with the same estimate for the time-acceleration factor; but instead of using a fixed boost potential, $\Delta V(\boldsymbol{r})$ in our recipe is temperature dependent and iteratively determined, based on $\rho(\boldsymbol{A})$, because the predetermination of a fixed effective boosting function is a hard task in general. For the choice of $\boldsymbol{A}$, our method is general as in metadynamics,[10] possibly with additional CV choices such as the Eshelby ellipsoid strain;[8] but unlike metadynamics we avoid the use of fixed Gaussian potentials, by resorting to a smooth histogram estimation approach that essentially "merges" the Gaussian potentials by a density-field estimator, where advanced mathematical treatment[11,12] is possible that gives a smoother and faster-to-evaluate $\Delta V(\boldsymbol{r})$.

Consider collective variables $\boldsymbol{A}$ which can be the bond length,[7] bond angle, atomic strain,[8] etc., that characterize a N-particle system. In a canonical ensemble ($\beta \equiv 1/k_{\mathrm{B}}T$) described by the Hamiltonian $\mathcal{H} = V(\boldsymbol{r}) + K(\boldsymbol{p})$, where $\boldsymbol{r}$ and $\boldsymbol{p} \equiv \{\boldsymbol{p}_1, \ldots, \boldsymbol{p}_N\}$ are the positions and momenta, the probability density $\rho(\hat{\boldsymbol{A}})$ of these collective variables is

$$\rho(\hat{\boldsymbol{A}}) = \frac{\int \cdots \int \delta(\boldsymbol{A}(\boldsymbol{r}) - \hat{\boldsymbol{A}}) \exp(-\beta\mathcal{H}) d\boldsymbol{r}\, d\boldsymbol{p}}{\int \cdots \int \exp(-\beta\mathcal{H}) d\boldsymbol{r}\, d\boldsymbol{p}}. \tag{2}$$

The coarse-grained free-energy surface $F(\boldsymbol{A})$ is

$$F(\boldsymbol{A}) = -k_{\mathrm{B}} T \ln \rho(\boldsymbol{A}). \tag{3}$$

If we add the following boost potential to Hamiltonian, $\boldsymbol{A}$ should have a flat histogram[13] in a canonical ensemble:

$$\Delta V(\boldsymbol{r}) \equiv \Delta V(\boldsymbol{A}(\boldsymbol{r})) = \Delta V(\boldsymbol{A}) = k_{\mathrm{B}} T \ln \rho(\boldsymbol{A}), \tag{4}$$

which means no ergodicity-breaking traps. The above is similar to the idea of the multicanonical ensemble Monte Carlo and MD.[14,15]

In practice it is impossible to obtain $\rho(\boldsymbol{A})$ because of the finite sampling in MD: All we have are discrete samples $\{\hat{\boldsymbol{A}}^k \equiv \boldsymbol{A}(\boldsymbol{r}(k\Delta t))\}$, where Δt is the MD time step and $k = 1 \ldots K$.

Using sophisticated density-field estimators[11,12] with better performance than straightforward Gaussian smearing, we can map the discrete data $\{\hat{\boldsymbol{A}}^k\}$ to $\rho(\boldsymbol{A})$, a smooth histogramic representation which closely resembles $P(\boldsymbol{A})$ in some parts of $\boldsymbol{A}$ space. Then we can define the boost potential $\Delta V(\boldsymbol{A}(\boldsymbol{r}))$ as

$$\Delta V(\boldsymbol{A}) = \begin{cases} k_{\mathrm{B}}T \ln \dfrac{\rho(\boldsymbol{A})}{\rho_{\min}}, & \rho(\boldsymbol{A}) \geqslant \rho_{\min}, \\ 0, & \rho(\boldsymbol{A}) < \rho_{\min}, \end{cases} \tag{5}$$

with $\rho_{\min}$ chosen such that the cumulative probability outside of the truncation is, say, $P_{\mathrm{cut}} = 5\%$. We note that in (5), the normalization of $\rho(\boldsymbol{A})$ is immaterial (so we do not need to worry about the height scale of the histogram), but the practically important parameter is P_{cut}.

The boost potential induces a fictitious force $\boldsymbol{F}_i^{\mathrm{boost}}$ on particle i:

$$\boldsymbol{F}_i^{\mathrm{boost}} = -\frac{\partial(\Delta V(\boldsymbol{A}))}{\partial \boldsymbol{r}_i} = -\frac{\partial(\Delta V(\boldsymbol{A}))}{\partial \boldsymbol{A}} \frac{\partial \boldsymbol{A}}{\partial \boldsymbol{r}_i}. \tag{6}$$

We should note that this method can also be applied to the problems involving supercell shape change. For example, by taking collective variable of supercell shape matrix $\boldsymbol{H}$ and performing NPT or $N\sigma T$ ensemble MD, we can evaluate the smooth histogram of $\boldsymbol{H}$ fluctuations and accelerate supercell deformation. In this case, in addition to the fictitious force on the internal coordinates of atoms, a fictitious stress tensor will also appear, which can be evaluated by taking a derivative of the boost potential with respect to the strain due to change of $\boldsymbol{H}$.[16]

If the free-energy barrier between two local minima i and j is sufficiently higher than $k_{\mathrm{B}}T$, then within a K-step MD simulation, the dividing surface between basin i and j is unlikely to be visited, in which case (5) should give

$$\Delta V(\boldsymbol{A}) = 0 \tag{7}$$

on the dividing surface. Then, according to the hyperdynamics theorem,[5] the relationship between the transition period $t_{i\to j}^{\mathrm{boost}}$ from state i to j in accelerated MD calculations and the actual transition period $t_{i\to j}$ can be expressed as

$$t_{i\to j} = t_{i\to j}^{\mathrm{boost}} \langle \exp[\beta \Delta V(\boldsymbol{A})] \rangle. \tag{8}$$

The entire algorithm for the adaptive-boost (AB) method is as follows. First, MD simulation in the canonical ensemble is performed for K time steps to obtain the initial distribution $\rho^{(0)}(\boldsymbol{A})$. If no state transition occurs during this zeroth MD calculation of K steps, the boost energy $\Delta V^{(1)}(\boldsymbol{A})$ is calculated by substituting $\rho^{(0)}(\boldsymbol{A})$ in (5). Next, $\Delta V^{(1)}(\boldsymbol{A})$ is added to the original $V(\boldsymbol{r})$ to carry out the first accelerated MD calculations, again in K steps. Then, $\rho^{(1)}(\boldsymbol{A})$ is obtained. If no state transition occurs during the first accelerated MD run, $\rho^{(1)}(\boldsymbol{A})$ is substituted in (5) to calculate the second boost potential $\Delta V^{(2)}(\boldsymbol{A})$, which is to be added onto $\mathcal{H} + \Delta V^{(1)}$. Such adaptive and cumulative boost operations are repeated until the state transition occurs during the Lth accelerated MD calculation. The total boost potential used in the Lth accelerated MD run is

$$\Delta V_{\mathrm{total}}^{L}(\boldsymbol{A}) = \sum_{l=1}^{L} \Delta V^{(l)}(\boldsymbol{A}), \tag{9}$$

and therefore the time acceleration is evaluated in (8) using the above $\Delta V(\boldsymbol{A}) = \Delta V_{\mathrm{total}}^{L}(\boldsymbol{A})$. Certain choices of mathematical representation[11,12] could allow "merging" of the log-histogramic terms on the right-hand side of (9) to give smoother and faster-to-evaluate $\Delta V(\boldsymbol{A}) = \Delta V(\boldsymbol{A}(\mathbf{r}))$ than simple summations of Gaussians.

Near the transition, it may be desirable to apply a "braking" procedure

$$\Delta V_{\mathrm{total}}^{L}(\boldsymbol{A}) = \sum_{l=1}^{L_{\mathrm{P}}-1} \Delta V^{(l)}(\boldsymbol{A}) + \sum_{l=L_{\mathrm{P}}}^{L} \alpha_l \Delta V^{(l)}(\boldsymbol{A}), \tag{10}$$

where a scaling factor α, $0 \leqslant \alpha_l < 1$, is used for $l \geqslant L_{\mathrm{P}}$, with L_{P} determined by a previous run without braking, in a "hit-back up 1 step-and-continuously brake" maneuver. If a sufficient number of adaptive-boost steps are implemented successively without transition, $-\Delta V_{\mathrm{total}}^{L}(\boldsymbol{A})$ will become approximately a replica of the free-energy surface $F(\boldsymbol{A})$. In the present method, it is not necessary to define the shape of the boost potential in advance.[5,7,8]

III. DENSITY-FIELD ESTIMATORS

An adaptive-boost approach was also used in metadynamics[9] by adding the Gaussian boost potentials incrementally. However, the advantage of the present recipe is that we are not tied to any particular functional form such as the Gaussian, which is arbitrary. It is known in the electronic-structure calculation community that Gaussian smearing is a primitive way to obtain the density of states, and many sophisticated density-field estimators such as Refs. 11 and 12 already exist that offer many practical advantages: (a) smoothness, (b) more efficient to evaluate, (c) analytically addable for operations in (9), for instance, using a spline-fitted representation, and (d) analytically differentiable for operation in (6).

In the present paper, if just one collective variable is used, the following recipe[12] is employed to estimate the one-dimensional smooth histogram. We define a discrete density function on $x \in [0, 2\pi)$,

$$\hat{\rho}(x) \equiv \sum_{k=1}^{K} \delta(x - \hat{x}^k), \tag{11}$$

where $x \equiv 2\pi[1/2K + (1 - 1/K)(A - \hat{A}^{\min})/(\hat{A}^{\max} - \hat{A}^{\min})]$, $\hat{x}^k = 2\pi[1/2K + (1 - 1/K)(\hat{A}^k - \hat{A}^{\min})/(\hat{A}^{\max} - \hat{A}^{\min})]$, $\hat{A}^{\max} = \max_{1\leqslant k\leqslant K} \hat{A}^k$, and $\hat{A}^{\min} = \min_{1\leqslant k\leqslant K} \hat{A}^k$, and a corresponding cumulant function

$$c(x) \equiv \int_0^x \hat{\rho}(x')dx'. \tag{12}$$

Define a residual function $R(x)$,

$$R(x) = c(x) - \frac{Kx}{2\pi}. \tag{13}$$

Here $R(x)$ is a periodic function and can be approximated by

$$R(x) \approx \tilde{R}(x) = \sum_{n=1}^{M} \{a_n[\cos(nx) - 1] + b_n \sin(nx)\}, \tag{14}$$

with a least-squares fit[12] and then smooth histogram can be obtained by taking the derivative of $\tilde{c} \equiv \tilde{R}(x) + Kx/2\pi$,

$$\rho(x) = \sum_{n=1}^{M} \{-na_n \sin(nx) + nb_n \cos(nx)\} + \frac{K}{2\pi}. \quad (15)$$

If more than one collective variable is used, we need to estimate multidimensional smooth histogram. In such cases, we employ the following density-field estimator based on the maximum-entropy method with a polynominal basis set.[11] In L dimensions, the maximum-entropy density field is

$$\rho(\boldsymbol{A}) \equiv \exp\left(- \sum_{\boldsymbol{n}} \lambda_{\boldsymbol{n}} \psi_{\boldsymbol{n}}(\boldsymbol{A}) \right), \quad (16)$$

where $\boldsymbol{n} = [n_1, n_2, \ldots, n_L]$, and

$$\psi_{\boldsymbol{n}}(\boldsymbol{A}) = \psi_{n_1}(A_1)\psi_{n_2}(A_2)\cdots\psi_{n_L}(A_L), \quad (17)$$

$\psi_{n_i}(A_i) = A_i^{n_i}$ $(i = 1,2,\ldots,L)$ and $\lambda_{\boldsymbol{n}}$ is the Lagrange multiplier. $\{\lambda_{\boldsymbol{n}}\}$ can be determined by numerically solving

$$\int \psi_{\boldsymbol{m}}(\boldsymbol{A}) \exp\left(- \sum_{\boldsymbol{n}} \lambda_{\boldsymbol{n}} \psi_{\boldsymbol{n}}(\boldsymbol{A}) \right) d\boldsymbol{A} = \sum_{k=1}^{K} \psi_{\boldsymbol{m}}(\hat{\boldsymbol{A}}^k), \quad \forall \boldsymbol{m} \geqslant 0, \quad (18)$$

using, for instance, the Newton-Raphson method.[11] Obviously, when the moments on the right-hand side are updated by the new data points added, we could use the previous $\{\lambda_{\boldsymbol{n}}\}$ as a guess solution, and take advantage of the quadratic convergence property of the Newton-Raphson method to reach a unique maximum-entropy density-field solution.

IV. APPLICATIONS

In this section we will use the AB method to investigate the transport of carbon in bcc iron across a wide range of temperatures, comparing bulk lattice diffusion with dislocation core diffusion.

A. Carbon diffusion in bcc iron lattice

To apply the AB method to a real problem, we first evaluated carbon atom diffusion in bcc Fe. It is known that C atoms exist at the octahedral sites of the Fe lattice and diffuse between adjacent O sites[1] (Fig. 1). Carbon diffusivity at around room temperature is about 10^{-20} cm^2/s,[17] and therefore the direct monitoring of the C diffusion using conventional MD is impossible.

A supercell in which one C atom was inserted in an α-Fe lattice comprising 432 atoms ($6 \times 6 \times 6$ bcc unit cells) was used as the calculation model. An embedded-atom model (EAM) potential of the Fe-C system[18] was used. The Nosé-Hoover method[19,20] was used for the generation of the canonical ensemble. The supercell dimensions were adjusted so that the internal stress is zero and were fixed during the MD runs. In this model, the activation potential energy barrier for a C atom jump between O sites was calculated to be 0.86 eV by using the nudged elastic band (NEB) method.[21] This value was just 1.1 meV higher than that calculated using a $10 \times 10 \times 10$ supercell, indicating that the supercell used in the present study were sufficiently large. The collective variable was set to be the

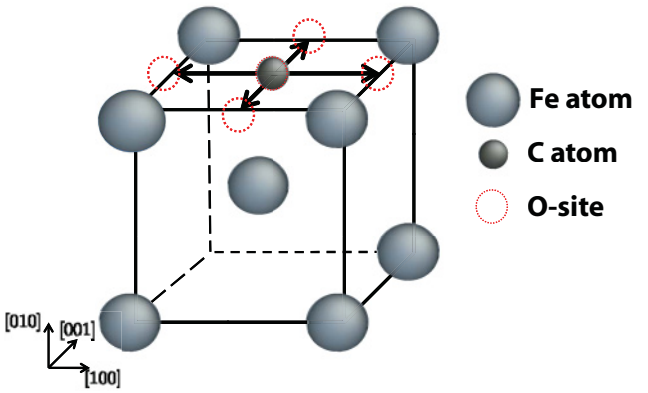

FIG. 1. (Color online) Schematics of C atom hops between adjacent O sites in α-Fe.

projected distance of C along the [100] direction relative to the center of mass of all Fe atoms, $r^{\mathrm{C}}_{[100]}$. That is, hopping of C to the adjacent two O site in the [100] direction would be accelerated. $\rho(r^{\mathrm{C}}_{[100]})$ was represented by using the one-dimensional density operator with $M = 10$. The number of MD steps was set to be $K = 10^4$ (at $T = 500$, 600 K), $K = 10^5$ (at $T = 300$ and 400 K), and $K = 10^6$ (at $T = 200$ K), with $\Delta t = 2$ fs. The boost potential ΔV in each adaptive-boost step (without braking) at 300 K is shown in Fig. 2. At 300 K, the state transition occurs during the third accelerated MD run. Using the resultant $\rho^{(3)}(\boldsymbol{A})$ and the corresponding $\Delta V^4_{\mathrm{total}}$, one can estimate the overall profile of the free energy during C atom migration between adjacent O sites at 300 K.

Next, we calculated the diffusivity based on the frequency of the C atom jump between adjacent O sites at each temperature. The average C atom jump frequency $\bar{\nu} = \bar{t}^{-1}_{\mathrm{O}\to\mathrm{O}}$ can be calculated from the average period required for jump between adjacent O sites, $\bar{t}_{\mathrm{O}\to\mathrm{O}}$. $\bar{t}_{\mathrm{O}\to\mathrm{O}}$ was obtained for five jump events between adjacent O sites, and then divided by 2 to take into account the fact an O site is surrounded by four

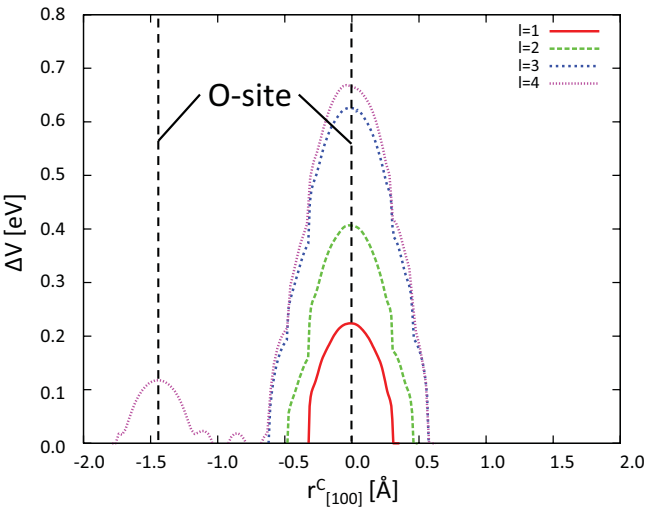

FIG. 2. (Color online) Boost energy $\Delta V^l_{\mathrm{total}}$ $(l = 1,2,3,4)$ used in lth accelerated MD runs at $T = 300$ K.

TABLE I. Acceleration factor at each temperature.

Temperature (K)	$\bar{t}_{O\to O}$ (ns)	$\bar{t}^{boost}_{O\to O}$ (ns)	$\bar{t}_{O\to O}/\bar{t}^{boost}_{O\to O}$
200	1.48×10^{16}	1.02×10^{-1}	1.45×10^{17}
300	3.24×10^{8}	5.64×10^{-2}	5.72×10^{9}
400	7.08×10^{4}	8.22×10^{-2}	8.78×10^{5}
500	2.48×10^{2}	8.12×10^{-3}	3.07×10^{4}
600	4.64	4.72×10^{-3}	9.78×10^{2}

equivalent O sites, two in [100] and two in [001], illustrated in Fig. 1. The diffusivity D is given by

$$D = \tfrac{1}{6}\bar{\nu}d^2, \tag{19}$$

where $d \approx 1.44$ Å is the distance between adjacent O sites. Table I shows the average jump period at each temperature, as calculated using (8). At 200 K, the time-acceleration factor we obtained is 1.45×10^{17}.

Figure 3 shows the temperature dependence of the diffusivity obtained by the AB method for $T = 200$–600 K and by conventional MD for $T = 600$–800 K. The calculation results are in good agreement at 600 K. Furthermore, the AB results match well with the experimental measurements. The activation enthalpy for diffusion is 0.90 eV, as calculated from the slope of the linear least-squares approximation of the accelerated and normal MD calculation results plotted for the temperature range 200–800 K. This value is consistent with the experimental values of 0.77–0.90 eV, and the density functional theory (DFT) calculation result of 0.86 eV.[18]

Next, we adopted three CVs $\boldsymbol{A} = \{r_C^{[100]}, r_C^{[010]}, r_C^{[001]}\}$ to perform accelerated MD calculations with a greater number

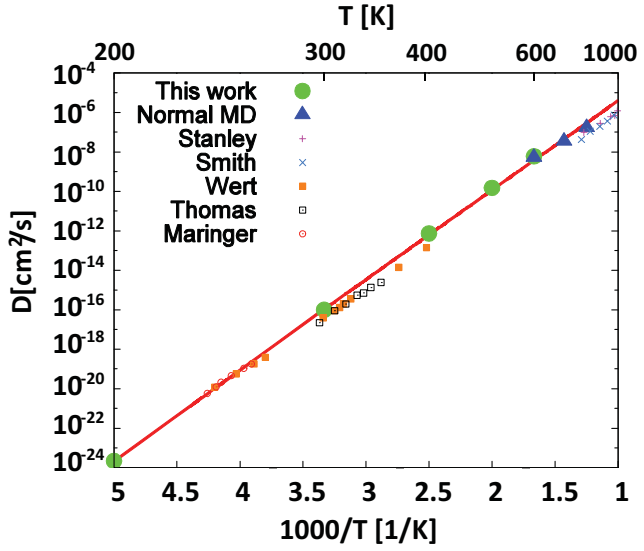

FIG. 3. (Color online) Temperature dependence of C diffusivity in α-Fe. Solid circles and solid triangles indicate the diffusivity calculated by the adaptive-boost method and conventional MD method, respectively. The line was calculated from these plots by using the least-squares method. Other plots indicate experimental values (Refs. 22–26).

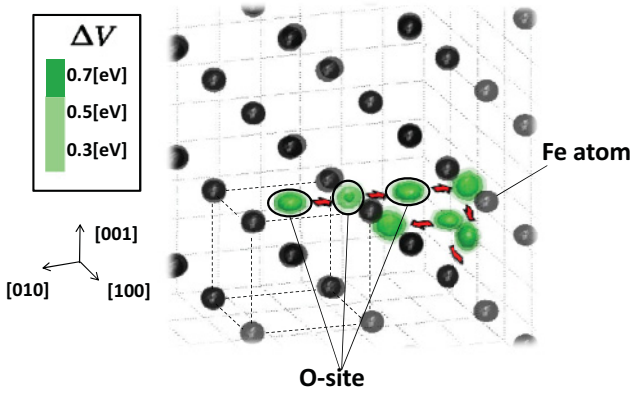

FIG. 4. (Color online) Boost energy isosurface of ΔV^{20}_{total} at 400 K. Black clouds indicate the positions of Fe atoms. Arrows indicate the C atom jump sequence.

of degrees of freedom. $\rho(\boldsymbol{A})$ was represented using the polynominal basis density-field estimator with $L = 3$ and $1 \leqslant n_i \leqslant 5$ $(i = 1,2,3)$. The temperature was set to 400 K. Figure 4 shows the boost energy isosurface for a boost energy of ΔV^{20}_{total}. A C atom at a certain O site tends to move within the plane in the direction of the four equivalent O sites adjacent to the C-atom-containing site and not in the direction perpendicular to the plane. Therefore, ΔV has a penny shape that is distorted in the in-plane directions. In this case, we calculated D from the changes in the C atom's three-dimensional spatial coordinates, by using the Einstein equation

$$D = \lim_{t\to\infty} \frac{1}{6t}\langle|\boldsymbol{r}_C(t) - \boldsymbol{r}_C(0)|^2\rangle. \tag{20}$$

We tracked the C atom motion during 3.0×10^6 ns by performing accelerated MD calculations and calculated D from (20) to be 4.47×10^{-13} cm^2/s. This value was consistent with that obtained at 400 K for one degree of freedom (shown in Fig. 3), $D = 4.88 \times 10^{-13}$ cm^2/s.

B. Comparison with hyperdynamics

We also followed the original hyperdynamics method[5] to calculate the carbon diffusivity at 400 K, for comparison with the AB method. The boost energy in hyperdynamics $\Delta V(\boldsymbol{r})$ is defined as follows:[5]

$$\Delta V(\boldsymbol{r}) = \Delta V^{\cos}(\boldsymbol{r}) + \Delta V^{\Delta\epsilon}(\boldsymbol{r}), \tag{21}$$

where

$$\Delta V^{\cos}(\boldsymbol{r}) = \frac{h}{2}\left[1 + \epsilon_1 \Big/ \left(\epsilon_1^2 + g_{1p}^2/d^2\right)^{1/2}\right] \tag{22}$$

and

$$\Delta V^{\Delta\epsilon}(\boldsymbol{r}) = \begin{cases} a[1 - 3q^2 + 2q^3], & q \leqslant 1, \\ 0, & q > 1. \end{cases} \tag{23}$$

The ϵ_1 and ϵ_2 are the two lowest eigenvalues of the Hessian matrix; $H_{ij}(\boldsymbol{r}) = \partial^2 V(\boldsymbol{r})/\partial x_i\, \partial x_j$ (x_i is a component of vector $\boldsymbol{r}$) and $q = (\epsilon_2 - \epsilon_1)/\Delta\epsilon$. g_{1p} is the projection of the gradient vector, $\boldsymbol{g} = \partial V(\boldsymbol{r})/\partial \boldsymbol{r}$, onto the lowest-eigenvalue eigenvector of the Hessian matrix. We use steepest-descent minimization

TABLE II. Carbon diffusivity at 400 K calculated by hyperdynamics with different $h(=a)$. No jumps were observed for $h \leqslant 0.25$ eV within 3000 hyperdynamics steps.

$h(=a)$ (eV)	D (cm^2/s)
0.1	
0.2	
0.25	
0.28	8.66×10^{-12}
0.3	4.51×10^{-12}
0.35	1.50×10^{-13}
0.4	1.02×10^{-14}
Exp. (Ref. 24)	1.41×10^{-13}
AB method	4.47×10^{-13}

to find ϵ_1, ϵ_2, and g_{1p}.[5] d and $\Delta\epsilon$ were set to be $d = 0.6$ Å and $\Delta\epsilon = 0.1$ eV, respectively. The parameters h and a, which determine the boost potential height, should be carefully chosen to have effective acceleration. We simply take $h = a$, and perform a 3000-step hyperdynamics run using different boost scales $h(=a)$. Computational wall-clock time for the 3000-step hyperdynamics run with, say, $h = 0.3$ eV was ten times longer than the 3-CV AB MD run. Calculated carbon diffusivities by using the Einstein equation are listed in Table II. For lower h ($\leqslant$0.25 eV), no carbon jump between adjacent O sites was observed within 3000 hyperdynamics steps. For higher h (=0.4 eV), diffusivity is significantly underestimated because of overboost which violates the assumptions of hyperdynamics (saddle points cannot be boosted; one cannot transform an uphill energy pathway to downhill, or even too shallow an uphill energy pathway so that the transition-state rate theory starts to break down). Thus, the efficiency of hyperdynamics strongly depends on the parameters h,a. However, defining these parameters in advance is not an easy task when the free-energy surface is totally unknown.

A possible strategy to perform accelerated MD simulations more efficiently is to hybridize between "free-form" AB and "fixed-form" hyperdynamics in the following way. At the beginning, when nothing is known about the system, one could run AB to bootstrap the bias potential form ΔV (now expressed in analytical polynomials instead of the sum of Gaussians) for this particular atomic environment. One could develop an automated computational geometry algorithm to classify the local geometry as "carbon at lattice O site," and associate this geometrical classifier with ΔV in a database. Next, one could perform AB calculation for carbon inside the dislocation core (to be shown next), carbon in a phase boundary, etc., to expand the database: For each typical atomic environment, one stores the corresponding AB-bootstrapped ΔV in the database. The highly compact form of ΔV in the polynomial basis would allow efficient storage. Such a bootstrapped $\{\Delta V\}$ database not only allows one to visualize the physics of diffusion, but would also accelerate subsequent simulations in the following way. For instance, when we simulate more complex thermomechanical processes where thousands of diffusional hops need to happen for the microstructure to evolve significantly,[27] one could first try to match the local atomic environment with those stored in the database. If a highly matching environment is found (after considering translational and rotational transforms), one could use the stored ΔV form (probably somewhat scaled in amplitude and arguments) as the initial boost potential, without the bootstrapping from zero. With such "fixed-form" ΔV from the catalog as the initial guess, one could still perform AB on top of it, as AB is a highly robust algorithm and can stop and restart arbitrarily, to compensate for the small but finite difference with the database environment. This unique ΔV may be further stored in the database along with the alternate environment. This way, one may be able to accelerate simulation of diffusive processes in inhomogeneous materials, where the stress field and local chemistry may modulate diffusion.[27]

C. Carbon diffusion near the edge dislocation core in bcc iron

In this section, we apply the AB method to a more complex problem, carbon atom diffusion inside the edge dislocation core in bcc Fe. The free-energy profile was previously unknown. An α-Fe 3960-atom simulation cell is used, which comprises six $(11\bar{2})$ atomic layers with a periodic condition in $[11\bar{2}]$, having one edge dislocation along $[11\bar{2}]$ at the center of the layers and one interstitial carbon atom at a stable site in the dislocation core (dashed circle in Fig. 5). The surface atoms in $(\bar{1}10)$ and (111) were fixed after relaxation of the initial atomic structure.

First, we performed normal MD at 200 K for 3.8 ns (1.9×10^5 MD steps) without any boost. Figure 5 indicates the carbon atom trajectory for 3.8 ns. After a while the carbon atom was trapped in a stable site in the dislocation core which corresponds to the site labeled "c" in Fig. 6(b), and did not escape from "c" within a time duration of 3.8 ns.

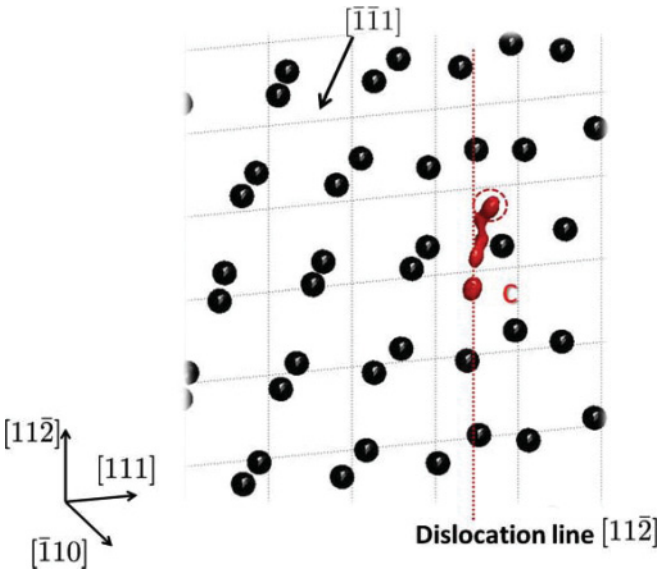

FIG. 5. (Color online) Trajectory of the C atom during 3.8 ns (1.9×10^5 MD steps) near the dislocation core at 200 K estimated by normal MD. Black clouds indicate the positions of the Fe atoms. The vertical dotted line and dashed circle indicate the dislocation line and initial position of the C atom, respectively.

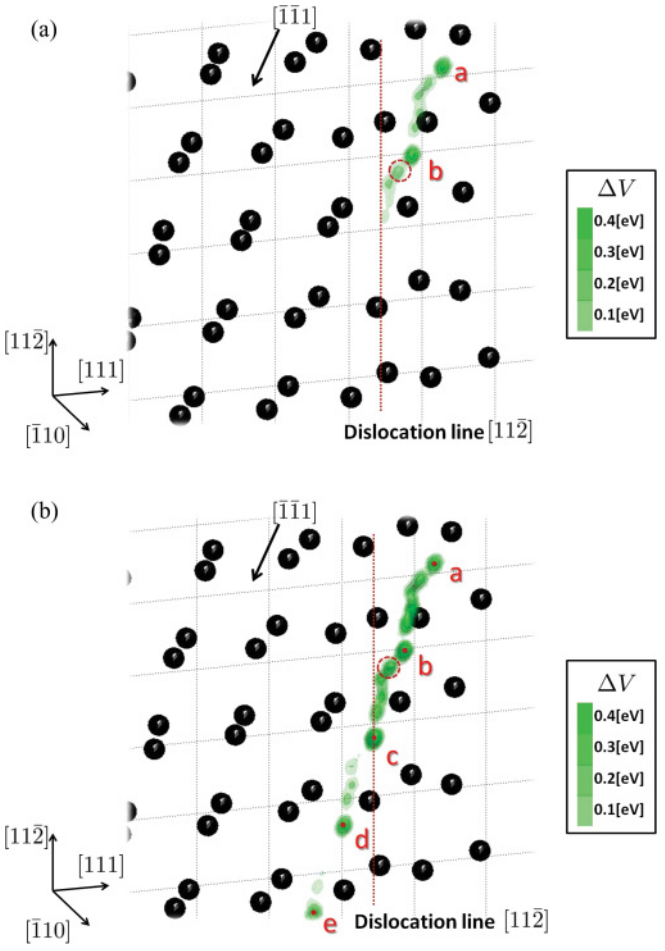

FIG. 6. (Color online) Boost energy isosurfaces of (a) $\Delta V^{7}_{\text{total}}$ and (b) $\Delta V^{19}_{\text{total}}$. Black clouds indicate the positions of the Fe atoms. The vertical dotted line and dashed circle indicate the dislocation line and the initial position of the C atom, respectively. The labels a–e indicate the long-stay sites. The small red dots in (b) indicate the center of the long-stay sites.

Next, we performed an accelerated MD calculation using the AB method. The same initial atomic arrangement was used as that of the previous normal MD calculation. We chose CVs $\boldsymbol{A} = \{r_{\text{C}}^{[111]}, r_{\text{C}}^{[1\bar{1}0]}, r_{\text{C}}^{[11\bar{2}]}\}$. The temperature was set to 200 K. The number of MD steps was set to be $K = 10^5$. $\rho(\boldsymbol{A})$ was represented using the polynominal basis density-field estimator with $N = 3$ and $1 \leqslant n_i \leqslant 5$ $(i = 1,2,3)$. Figures 6(a) and 6(b) show the boost energy isosurfaces for boost energies of $\Delta V^{7}_{\text{total}}$ and $\Delta V^{19}_{\text{total}}$, respectively. We found long-stay sites [labeled a–e in Fig. 6(b)] aligning in the $[\bar{1}\bar{1}1]$ direction, which is not entirely parallel with the dislocation line direction $[11\bar{2}]$, and several short-stay sites in between the neighboring long-stay sites. This site alignment is consistent with the MD analysis at high temperature by Tapasa *et al.*[28] We calculated the average time for C atom migration between the long-stay sites (b → a, a → b, c → d, d → e) from Eq. (8) to be 0.53 s. This physical time scale of carbon migration is significantly longer than the accessible time scale of normal MD. We also calculated activation free energies between the long-stay sites to be 0.3–0.4 (eV) and between the short-stay sites to be 0.1–0.2 (eV) from the AB-bootstrapped ΔV.

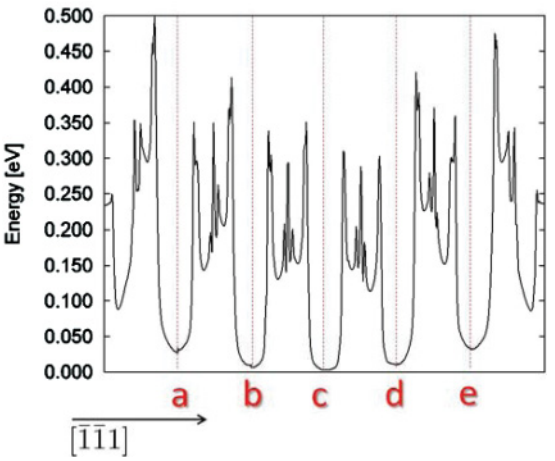

FIG. 7. (Color online) Potential energy change along the minimum energy path connecting the long-stay sites a–e.

Then, to validate the details of the potential energy change along the diffusion path, we employed the NEB analysis.[29] Figure 7 shows the potential energy change along the minimum energy path connecting the sites a–e that were found in the accelerated MD. We can observe "long-stay sites" and several "short-stay sites" between the long-stay sites, and these potential barrier heights are consistent with the free-energy barrier heights obtained from the accelerated MD.

We have also calculated the carbon atom trap energy in the edge dislocation core to be 0.96 eV, which is the energy difference between the "c" site in the edge dislocation core and the O site in the regular bcc lattice. This trap energy means that the edge dislocation is a path for C atom diffusion in bcc Fe. We should note that since the dislocation line is not parallel to the local direction of carbon diffusion, coordinated motions of dislocation glide and carbon diffusion are necessary for a continuous carbon diffusion along the edge dislocation.[28]

V. CONCLUSION

In summary, a smooth histogram-based adaptive accelerated MD method is developed to model rare microscopic events. Single-particle displacement is found to be a sufficient "collective variable" for boosting carbon interstitial diffusion, where the adaptive-boost potential takes on a single-particle effective potential form based on finite-temperature occupation, which philosophically is the antithesis of the Einstein vibration model of solids and destabilizes Einstein-Debye-Waller vibrations around local minima. The time-acceleration factor achieved is as high as 1.45×10^{17} in adaptive-boost simulations at 200 K, allowing one to "observe" diffusion in a dynamical simulation that may even go beyond the reach of normal laboratory experiments. Furthermore, we demonstrate carbon diffusion inside the edge dislocation core in bcc Fe by using AB MD simulation, and shows that the carbon atom encounters significantly lower migration barriers (0.3–0.4 eV) than in the lattice (0.90 eV), as well as enjoys a significant segregation enrichment benefit characterized by the trap energy of 0.96 eV. Thus, even with moderate dislocation density in a ferritic steel grain, there should be a critical

temperature below which carbon transport by dislocation core diffusion dominates over lattice diffusion.

ACKNOWLEDGMENTS

This study was partially supported by a Grant-in-Aid for Scientific Research (B), 20360055 and (A), 23246025, Scientific Research on Innovative Area, 22102003, Challenging Exploratory Research, 22656030, JST under Collaborative Research Based on Industrial Demand (Heterogeneous Structure Control). J.L. was supported by NSF under Grants No. CMMI-0728069, No. DMR-1008104, and No. DMR-1120901, and AFOSR Grant No. FA9550-08-1-0325.

*ogata@me.es.osaka-u.ac.jp
†liju@mit.edu

[1] H. Mehrer, *Diffusion in Solids: Fundamentals, Methods, Materials, Diffusion-Controlled Processes* (Springer, Berlin, 2007).
[2] T. Huber, A. E. Torda, and W. F. Vangunsteren, J. Comput.-Aided Mol. Des. **8**, 695 (1994).
[3] H. Grubmuller, Phys. Rev. E **52**, 2893 (1995).
[4] O. Engkvist and G. Karlstrom, Chem. Phys. **213**, 63 (1996).
[5] A. F. Voter, Phys. Rev. Lett. **78**, 3908 (1997).
[6] A. Laio and M. Parrinello, Proc. Natl. Acad. Sci. USA **99**, 12562 (2002).
[7] R. Miron and K. Fichthorn, J. Chem. Phys. **119**, 6210 (2003).
[8] S. Hara and J. Li, Phys. Rev. B **82**, 184114 (2010).
[9] A. Laio and F. Gervasio, Rep. Prog. Phys. **71**, 126601 (2008).
[10] M. Bonomi, D. Branduardi, G. Bussi, C. Camilloni, D. Provasi, P. Raiteri, D. Donadio, F. Marinelli, F. Pietrucci, R. A. Broglia, and M. Parrinello, Comput. Phys. Commun. **180**, 1961 (2009).
[11] J. Eapen, J. Li, and S. Yip, Phys. Rev. E **72**, 056712 (2005).
[12] J. Li, P. Kevrekidis, C. Gear, and I. Kevrekidis, SIAM Rev. **49**, 469 (2007).
[13] F. G. Wang and D. P. Landau, Phys. Rev. E **64**, 056101 (2001).
[14] B. Berg and T. Neuhaus, Phys. Lett. B **267**, 249 (1991).
[15] N. Nakajima, H. Nakamura, and A. Kidera, J. Phys. Chem. B **101**, 817 (1997).
[16] J. H. Wang, J. Li, S. Yip, S. Phillpot, and D. Wolf, Phys. Rev. B **52**, 12627 (1995).
[17] A. Lord Jr. and D. Beshers, Acta Metall. **14**, 1659 (1966).
[18] T. T. Lau, C. J. Först, X. Lin, J. D. Gale, S. Yip, and K. J. VanVliet, Phys. Rev. Lett. **98**, 215501 (2007).
[19] S. Nosé, J. Chem. Phys. **81**, 511 (1984).
[20] W. G. Hoover, Phys. Rev. A **31**, 1695 (1985).
[21] G. Henkelman, B. P. Uberuaga, and H. Jonsson, J. Chem. Phys. **113**, 9901 (2000).
[22] J. Stanley, Trans. Am. Inst. Min. Metall. Eng. **185**, 752 (1949).
[23] R. P. Smith, Trans. Am. Inst. Min. Metall. Eng. **224**, 105 (1962).
[24] C. Wert, Phys. Rev. **79**, 601 (1950).
[25] W. R. Thomas and G. M. Leak, Philos. Mag. **45**, 986 (1954).
[26] R. E. Maringer, J. Appl. Phys. **35**, 2375 (1960).
[27] J. Li, S. Sarkar, W. T. Cox, T. J. Lenosky, E. Bitzek, and Y. Z. Wang, Phys. Rev. B **84**, 054103 (2011).
[28] K. Tapasa, Y. Osetsky, and D. Bacon, Acta Mater. **55**, 93 (2007).
[29] G. Henkelman and H. Jónsson, J. Chem. Phys. **113**, 9978 (2000).